Journal Pre-proof

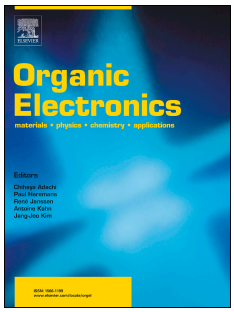

Ultrasensitive and low temperature gas sensor based on electrospun organic-inorganic nanofibers

Waseem Hittini, Yaser E. Greish, Naser N. Qamhieh, Mohamed A. Alnaqbi, Dagou Zeze, Saleh T. Mahmoud

PII: S1566-1199(20)30045-8

DOI: https://doi.org/10.1016/j.orgel.2020.105659

Reference: ORGELE 105659

To appear in: *Organic Electronics*

Received Date: 8 October 2019

Revised Date: 11 February 2020

Accepted Date: 12 February 2020

Please cite this article as: W. Hittini, Y.E. Greish, N.N. Qamhieh, M.A. Alnaqbi, D. Zeze, S.T. Mahmoud, Ultrasensitive and low temperature gas sensor based on electrospun organic-inorganic nanofibers, *Organic Electronics* (2020), doi: https://doi.org/10.1016/j.orgel.2020.105659.

This is a PDF file of an article that has undergone enhancements after acceptance, such as the addition of a cover page and metadata, and formatting for readability, but it is not yet the definitive version of record. This version will undergo additional copyediting, typesetting and review before it is published in its final form, but we are providing this version to give early visibility of the article. Please note that, during the production process, errors may be discovered which could affect the content, and all legal disclaimers that apply to the journal pertain.

© 2020 Published by Elsevier B.V.

An ISO 9001, 14001 and OSHA 18001 Certified.© Copyright. & Powered by : ASK-EHS Engineering & Consultants Pvt. Ltd.

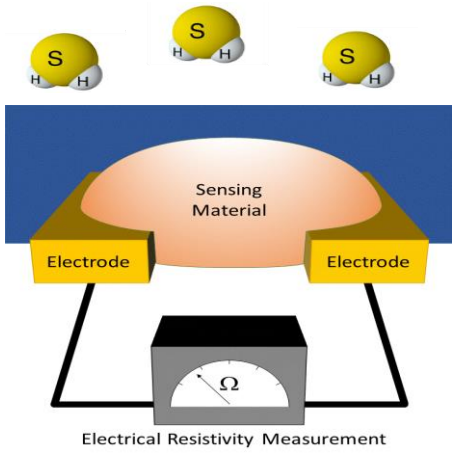

Electrical Resistivity Measurement

Copyright 2019 by CSIRO Cooper

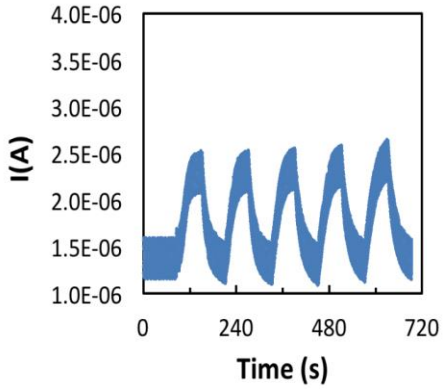

Journal Pre-proof

Ultrasensitive and Low Temperature Gas Sensor Based on Electrospun Organic-Inorganic Nanofibers

Waseem Hittini [a], Yaser E. Greish [b], Naser N. Qamhieh [a], Mohamed A. Alnaqbi [b], Dagou Zeze [d,e], Saleh T. Mahmoud [a,*]

[a] Department of Physics, UAE University, Al Ain, United Arab Emirates
[b] Department of Chemistry, UAE University, Al Ain, United Arab Emirates
[d] Department of Engineering, Durham University, Durham, United Kingdom
[e] ITMO University, St Petersburg, Russia (Visiting Professor)

Abstract

Organic-inorganic hybrid material is one of the most promising materials for high performance gas sensors due to its improved properties like high sensitivity, selectivity, fast response time, flexibility and low power consumption. This work presents ultrasensitive, selective and low operating temperature H_2S gas sensor. It is based on metal-oxide nanoparticles (NPs) embedded in organic semiconductor polymeric nanofibrous (NFs) membrane containing an ionic liquid (IL). In this context, high surface area Tungsten(VI) oxide- Polyvinyl alcohol (WO_3-PVA) nanofibrous composite sensor material with average diameter of 130 ± 20 nm were synthesized with controlled morphology and interconnectivity through an electrospinning technique. The obtained WO_3 NPs-containing PVA nanofibrous sensing material was evaluated for its ability as a potential sensor for H_2S gas at different operating temperatures and gas concentrations. Results demonstrated that the fabricated sensor is ultrasensitive and selective for H_2S gas and exhibit an excellent reproducibility, and long-term stability. Furthermore, the sensor showed adequate response in a humid environment. It was also shown that nanofibers' membrane porosity and thickness control the sensing performance. The optimum operating temperature of 40°C with a detection threshold as low as 100 ppb with a response time of 16.37 ± 1.42 s were achieved. This combined high sensitivity, fast response time and low operating temperature (low-power consumption) provides clear evidence of the sensor's potential to outperform existing devices, which could pave the way for a commercial exploitation.

Keywords: H_2S sensor; WO_3 nanoparticles; Semiconductor polymer; Nanofibers

Journal Pre-proof

1. Introduction

The increasing concern about environmental protection has resulted in continuous expansion in sensor development for hazardous gases detection. Hydrogen Sulfide (H_2S) is a colorless, highly flammable, extremely toxic, and explosive gas [1, 2]. It is produced as a by-product in petroleum and refining processes, sewer and wastewater treatment, pulp and paper processing, food processing, hot asphalt paving, textile manufacturing, landfills and mining [3-5]. Generally, workers in these industries face the risk of H_2S gas exposure. Although Wetchakun et al. [6] reported that H_2S exposure threshold limit value is 10 ppm, the Scientific Advisory Board on Toxic Air Pollutants (SAB-USA) reported that the acceptable ambient level of H_2S is at a lower range of 20-100 ppb [7]. Therefore, scientists and researchers have recently focused their efforts on developing H_2S gas sensors with low detection limit, fast response and low power consumption [8-18].

Organic materials have recently been designed as an effective approach to achieve cost-effective sensors with high performance. Conductive polymers and semiconducting materials are characterized by their ease of operation and fabrication, high sensitivity and low cost [15-17, 19]. It was also noted that conducting polymers have an enhanced affinity to gases, especially those that result in a change in their resistance [20-22]. On the other hand, semiconducting materials were found to change their electrical conductivity caused by adsorption and desorption of gases, a phenomenon that was first observed by Seiyama et al. in 1962 [18]. A number of metal-oxide semiconducting materials such as: In_2O_3 [23, 24], SnO_2 [25, 26], CuO [27, 28], WO_3 [29, 30], MoO_3 [31] and Fe_2O_3 [32, 33] were investigated as potential H_2S gas sensors. Among these oxide materials, WO_3 is an n-type metal-oxide with a band gap of 2.6-3.0 eV [34], a good surface morphology, active surface area and defect structure that boost its sensing properties.

Gas sensing applications are expected to undergo significant development due to the use and integration of nanomaterials in their device structures. The core advantage of the nano-scale structures, in the form of nanoparticles and nanofibers, is the large surface area to volume ratio compared to bulk materials. This feature leads the way towards more possibilities for creating new materials and facilitating chemical processes. Various types of nanomaterials were explored in this regard, such as thin films [35-37], nanofibers [38, 39], nanosheets [40, 41], nanowires [32, 42], nanocluster [43], quantum dots [44]. Among these various geometries, nanofibers (NFs) were found to possess a better sensitivity and selectivity for H_2S gas detection due to their large surface-to-volume ratio and high interconnected porosity [45].

Most recently, there has been an increasing interest in the fabrication of electronic devices based on hybrid structures that are made of organic and inorganic nanomaterials because of their distinguished properties such as power saving, size compactness and portability [46]. Their use for H_2S detection would help achieving the optimum enhancement of H_2S sensors in terms of sensitivity, selectivity, response time, low power consumption, easy fabrication, and flexibility. Hybrid organic-inorganic thin films made of semiconducting polymer, in which metal-oxides NPs were embedded, have been synthesized to detect H_2S gas at low concentrations. Results revealed an excellent performance in terms of sensitivity (10-25 ppm), fast response (20 s), operating temperature (80°C) and selectivity for H_2S gas at low temperatures [47-49]. On the other hand, Virji et al. [21] had reported that the addition of inorganic NPs to polymer NFs increased the sensitivity of the H_2S sensor. The advantage of the latter system is to combine the high surface area of both nanoparticles and nanofibers in order the maximize the possibilities of interaction between the adsorbed gas molecules and the sensor material. Moreover, recent studies investigated the effect of adding ionic liquids on the electrical

properties of insulating polymers. The results revealed that insulating polymers act as semiconducting materials when mixed with ionic liquid at specific ratios [50, 51]. An example of an environmentally-friendly ionic liquid is glycerol, which is believed to serve both as electrolytes and diffusion barriers [52].

Researchers usually use sacrificial polymeric materials, such as PVA, as templates for the containment of NPs, and to provide NPs-based sensor materials upon calcination [53, 54]. This is resulting in high activation energy of the developed sensors due to the high activation energy pf the prepared nanoparticles.

In the current study, PVA was used as a starting material for the development of a novel nanofibrous sensor membrane that contains WO_3 NPs, as a semiconducting sensor material, and glycerol, as an ionic liquid. Despite the continuous research in the area of fabrication of organic-inorganic gas sensors, the current study provides a novel formulation of organic nanofibers, inorganic nanoparticles and an ionic liquid to be used as a H_2S gas sensor. The performance of the prepared organic-inorganic nanofiber based sensor was thoroughly characterized and evaluated as a function of [WO_3], membrane thickness and sensing temperature. Throughout the obtained findings, optimization of the sensor fibrous membrane will be attempted.

2. Experimental

2.1. Preparation of Nanofibers composites

Tungsten oxide nano-powder (<100 nm), PVA (Mw ~61,000) and Glycerol (≥ 99.5%) were purchased from Sigma-Aldrich. A 10 wt% PVA solution was prepared by adding 1 g of PVA polymer to 10 mL of deionized water. The homogeneous PVA solution was further loaded with 5 vol% glycerol and 5, 7.5 and 10 wt% of WO_3 nano-powder. Each mixture was then exposed to vigorous stirring at 90°C until a clear homogenous solution was formed, followed by

cooling to room temperature. Each solution then filled into a 10 ml syringe with gauge 18 stainless steel needle to be electrospun into fibers. An electrospinning process was used at ambient conditions, and following a pre-determined set of parameters: spinning distance of 10 cm, an applied voltage of 12 kV applied between the needle tip and a grounded collector, and a constant flow rate of 0.5 ml/h was adjusted using an automatic syringe pump. The fiber density, hence membrane thickness, was controlled by varying the spinning process for 5, 7, and 9 hours, to study the effect of polymer fibers density on H_2S sensing. The obtained electrospun fibrous membranes were further dried at 60^{o}C for 24 hours to remove residual deionized water.

2.2. Material Characterization

A Shimadzu 6100 X-ray diffractometer with a Cu-Kα_1 radiation (λ = 1.54056 Å) was used to study the crystal structure of the as-received WO_3 NPs. The as-received WO_3 NPs and the as-prepared fibers' morphologies were investigated using scanning electron microscopy (SEM: JEOL, JSM- 5600). A DiameterJ software tool was used to analysis the SEM images in terms of fiber and pore size distributions [55]. In addition, an energy-dispersive X-ray spectrometer (EDX) was used to confirm the presence and homogeneity of the WO_3-PVA composite fibrous membranes. In order to determine the electrical and gas sensing properties of the prepared fibers, Keithley Instruments source measurement unit (KI 236) was utilized.

2.3. Sensor fabrication and Characterization

The device structure of sensor fabricated is shown in Fig. 1 and consists of three components: a copper sheet, sensing nanofiber material and a stainless-steel grid. The copper sheet (1.5 × 1.5 cm^2) was used as a bottom contact, and the stainless-steel grid (250 × 250 µm^2) as the top contact. A square piece (1 × 1 cm^2) of the composite NFs was cut and placed between the two contacts. A strong heat-proof squash tape was used to attach the three parts together. The

device was positioned on a heater plate inside a Teflon chamber fitted with 2 electrical feed-troughs to contact the bottom and top parts of the device. A detailed schematic diagram of the gas testing system is provided in Fig. 1. A mass flowmeter (Bronkhorst) was used to control the gases flow rate. H_2S gas was mixed with fixed proportion of dry air unless otherwise stated. With this arrangement, the developed sensors were subsequently exposed to H_2S gas inside the temperature-controlled Teflon chamber. The tests were conducted at different temperatures (20°C, 40°C and 60°C) under atmospheric pressure inside a fume hood. All tests were performed by applying a fixed bias of 2 V and the current was measured as a function of time at different H_2S concentrations. For each measurement, adequate number of samples were prepared and tested.

3. Results and discussion

3.1. Structural and morphological characteristics

XRD investigation of the as-received WO_3 NPs was carried out to confirm structural purity of the NPs. Fig. 2A indicates the presence of a monoclinic WO_3 phase, as compared with its JCPDS card number 83-0950 where all characteristic peaks were observed. No other phases were detected. In addition, the intense peaks observed reflect the high crystallinity of the prepared WO_3 NPs. However, the relative broadness of the peaks is attributed to their small size (nm) as shown in Fig. 2B, where nanoparticles of WO_3 and their agglomerates were observed. The average particle size of the as-received WO_3 was calculated using an imageJ software, and was found to be 13 ± 3 nm, which was further confirmed using a zetasizer measurement.

Fig. 3 A-C show the SEM micrographs of the PVA nanofibrous membranes containing 5 vol% IL and 5 wt% WO_3 NPs, made by electrospinning their respective solutions for 5, 7 and 9 hours, respectively. All composite nanofibers showed continuous, uniform and smooth surface

morphology. Moreover, their size distribution measured by Diameter J software, were also homogeneous, as evident from the fiber size distribution graphs shown in the insets of the SEM micrographs, with an average size of 140-200 nm. Extended spinning for 9 hours showed the formation of fibers with ribbon-like morphology, as shown ion Fig 3C. Extending the spinning time was also reflected in the pronounced increase in the thickness of the fibrous membranes showing thickness of 56.8, 173.5 and 210.6 µm for membranes made by spinning for 5, 7 and 9 hours, respectively. Accordingly, this resulted in a slight decrease of the interconnected porosity of the membranes to an average of 45%, as shown in Fig. 3D. A spinning time of 9 hours was accordingly selected as an optimum condition for studying the effect of varying the concentration of the WO_3 NPS in the membranes prepared thereafter. Fig. 4 shows the morphology of the prepared membranes containing 5, 7.5 and 10 wt% of WO_3 NPs. Figure 4A shows the morphology of a pristine PVA membrane for comparison, where fibers with a homogeneous size distribution and an average diameter of 116.4 nm were observed, as indicated from the fiber size distribution shown in the insert of Fig. 4A. In contrast, the SEM micrographs of PVA nanofibrous membranes containing 5, 7.5 and 10 wt% of WO_3 NPs shown in Fig. 4B-D show a noticeable change in the average fiber size and extent of ribbon formation with increasing the concentration of WO_3 NPs in the fibrous membranes. These results are in a good agreement with the data presented by Park et al. [56], where an increase of the diameter of PVA-montmorillonite-silver fibers was reported with increasing the content of Ag NPs, and was attributed to the increase in the viscosity of the solution with the addition of the NPs. It is a known fact that increasing the viscosity of the solution prior its electrospinning leads to a pronounced increase in the diameter of the produced fibers [57]. Consequently, the increase in the dimensions of the WO_3-containing PVA nanofibers led to a decrease in the porosity of the

membranes, as shown in Fig. 4E. Both thickness and porosity of the WO3-PVA fibrous membranes were believed to play an important role in the sensing efficiency of the produced membranes, as will be described later. Moreover, the presence of the WO3 NPs was further confirmed by an elemental analysis (EDS) of the fibrous membrane containing the highest concentration of WO_3 NPs (10 wt%), as shown in Fig. 4F. An optimum concentration of 7.5 wt% of WO_3 NPs in the PVA fibrous membranes was selected for studying the sensing characteristics of the prepared membranes.

A comparison between the thermal history of the as-received PVA pellets and the electrospun PVA nanofibers was carried out by thermogravimetric analysis (TGA), as shown in Fig. 5. The weight loss of both samples was measured over the temperature range 30-600°C. The decomposition of PVA beads takes place through three main events; at 250, 340 and 460^{o}C. These events are related to the dehydration (-H_2O) through the removal of the pending OH group and a neighboring H atom, while the second and third events are related to the degradation and decomposition (burn out) of the polymeric chains, respectively [58]. In contrast, the TGA thermogram of the PVA nanofibers took place through five events at 75, 180, 260, 360 and 480^{o}C. The first two events represent the removal of the weakly adsorbed water molecules at 75 and 180^{o}C, while the event at 260^{o}C is related to the removal of structural water molecules from the PVA polymeric chains. The last two events at 360 and 480^{o}C are related to the degradation and decomposition of the polymeric chains [58]. The detailed and early thermal history of the PVA nanofibers is attributed to its higher surface, which is a consequence of their nm-scale dimensions. However, the early thermal instability of the PVA NFs indicates their limited application as NPs-containing sensor membranes at temperatures below 75^{o}C to avoid the early

deterioration of the sensor material. These results are in agreement with previous findings where semiconducting polymers are used to detect H_2S gas in a temperature range of 20-80^oC [47-49].

3.2. Electrical properties

PVA nanofibrous membranes containing 7.5 wt% of WO_3 NPs and electrospun for 9 hours in addition to 5 vol% of the IL were used to investigate their electrical characteristics at various temperatures and concentrations of H_2S gas. Fig. 6A shows the I-V characteristics of nanofibrous membranes as measured at 20^oC, 40^oC and 60^oC. All I-V curves exhibited a degree of linearity, which became dominant at high temperature. Based on these results a bias voltage of 2 V was applied to measure the electrical current of the sensor in the linear part of I-V curve. The voltage point was chosen from the liner point in the I-V curve in order to avoid any current saturation. On the other hand, the nonlinear section of the I-V curves can be correlated to the charge carriers transport at the potential barrier formed between the PVA nanofibers and the WO_3 NPs entrapped within the nanofibers. Fig. 6B shows the natural logarithm of the resistance versus the reciprocal of temperature where the resistance decreases with increasing temperature. This phenomenon is attributed to the increase in the number of the free change carriers in the conduction band that were thermally excited. The resistance of the membranes, as depicted from the results of Fig. 6B, are therefore best fitted by the Arrhenius equation (1):

$$R = R_o e^{\frac{E_a}{K_B T}} \qquad \text{(Eq. 1)}$$

where, R is the sensor resistance, R_O is a pre-exponential factor, E_a is the activation energy, k_B is the Boltzmann constant and T is the temperature. The slope of the line in Fig. 6B was used to calculate the activation energy for the WO_3 NPs-containing PVA nanofibrous sensor membrane. An activation energy of 0.146 eV was found, which is lower than that of other WO_3–based sensors, e.g. CuO-functionalized WO_3 nanowires (E_a = 2.6 eV) [59]. Lower activation energy is highly desirable since it boosts the sensor's response and recovery time while decreasing the operating temperature [60].

3.3. Gas sensing properties

In addition to the variation of the proportion of WO_3 NPS in the PVA nanofibrous membrane and the spinning time, the gas sensing properties of the prepared nanofibrous membranes were also investigated as a function of the temperature and concentration of the H_2S gas. The fabricated nanofibrous sensor membranes were installed in a closed temperature-controlled Teflon chamber and exposed to different concentrations of H_2S gas. A fixed bias voltage of 2V was applied across the sensor's electrodes and the variation of the current was recorded as a function of time. The sensor response was calculated using equation 2,

$$S(\%) = \frac{I_g - I_a}{I_a} \times 100 \qquad \text{(Eq. 2)}$$

where S is the sensor response, I_a the reference current when the sensor is exposed to air and I_g the current measured when the sensor is exposed to the targeted H_2S gas mixture.

Fig. 7 represents a typical response curve for a PVA nanofibrous sensor membrane containing 7.5 wt% WO_3 and 5 vol% IL and electropsun for 9 hours when placed in a chamber containing H_2S gas with a concentration of 1 ppm at 20^{o}C and 100 ppm at 40^{o}C. The sensor membrane clearly shows a significant increase in the current as H_2S was introduced to the

chamber. Upon switching off the H_2S supply, the current drops back to its initial value. Moreover, it was found that the current of the sensor was changed in an identical manner through the five duty cycles displayed. In order to further evaluate the sensitivity of the currently optimized sensor towards lower concentrations of H_2S gas, the later was reduced to 100 ppb. However, no detection was observed. Accordingly, the temperature inside the chamber was raised to 40^{o}C, at which detection was observed, as shown in Fig 7B. Doubling the concentration of H_2S required the increase of the temperature inside the chamber to be 40^{o}C to maintain sensing efficiency, as shown in Fig 7B. This could be related to the enhanced activation of the sensor material in the presence of higher concentrations of the pollutant gas, as was previously shown in Fig. 6B. These results clearly demonstrate the reproducibility and reliability of the described nanofibrous sensor membranes.

The effect of increasing the thickness of the nanofibrous sensor membranes on their sensing efficiency was also studied as a function of the H_2S gas concentration, up to 10 ppm, and temperature, 40 and 60^{o}C. A lower concentration of 5 wt% for the WO_3 NPs in the sensor membranes was, therefore selected. Results are shown in Fig. 8, where the fibrous sensor membrane with the largest thickness; spun for 9 hours, was found to be capable of detecting as low as 1 ppm of H_2S gas at 40°C and 60°C, with an enhanced performance than fibrous sensor membranes with lower thicknesses. This could be attributed to the densification of the fibrous membranes caused by extending he spinning time, which was previously shown in Fig. 4E in terms of the decreased membrane porosity and the increased fiber size. The enhanced densification is believed to result in higher connectivity between the fibers and the WO_3 NPs entrapped within [45]. Accordingly, a thorough investigation of the sensing performance was

carried out using WO_3 NPs-containing PVA nanofibrous membranes that were made by spinning for 9 hours as a function of temperature and concentration of H_2S gas.

Fig. 9 A-C illustrates the effect of the operating temperature on the performance of the sensor, showing that the sensor response improved as the temperature was raised to 40°C, then decayed at higher temperatures (> 60°C). This could be related to the effect of raising the temperature on the structural characteristics of the PVA fibers as the temperature of measurement was elevated to a value closer to the first thermal event that was observed in the TGA thermogram of the PVA fibers (Fig. 5). On the other hand, the results shown in Fig. 9 A-C also indicate that the response of the WO_3 NPs-containing fibrous sensor was improved with increasing the proportion of the WO_3 NPs in the membranes up to to 7.5 wt%. This is attributed to the increase in the concentration of the active sites within the fibrous sensing membrane with the addition of WO_3 NPs [48], which boosts the sensor's performance. However, a noticeable decrease in the response of the WO_3 NPs-containing fibrous sensor was observed by increasing the content of the WO_3 NPs to 10 wt%. This could be related to a possible agglomeration of the WO_3 NPs within the fibers, which is a common problem faced during the dispersion of NPs in polymeric solutions. As a result, a loss of the high surface area of the NPS will take place, hence affect their sensing capability.

In brief, our investigation demonstrated that a PVA nanofibrous sensor membrane containing 7.5 wt% WO3, and 5 vol% IL and electrospun for 9 hours exhibit the highest performance at 40°C when compared with all other samples. Therefore, a maximum operating temperature of 40°C was used for the rest of the measurements. It should be mentioned that the sensor's response time for 1 ppm, which is defined as the time needed to achieve 90% of the response value, was found to be approximately 14.13 ± 2.29 s for the optimally selected WO_3

NPs-containing PVA nanofibrous sensor membrane, as shown in Fig. 9 D. This response time is shorter than that previously reported sensors (20 s) [48, 61, 62].

Accordingly, the long-term stability of the optimally fabricated sensor membrane was further evaluated by measuring the sensor response to the presence of 1 ppm of H_2S gas at 40°C for 21 days. Results are shown in Fig. 10A. The sensor exhibited an excellent stability with a minimal standard deviation of 2.59. On the other hand, the influence of humidity on the sensitivity of the optimally selected sensor membrane was also evaluated under 20-80% relative humidity. The sensor exhibits stable performance for relative humidity less than 40% as shows in Fig. 10 B. However, a decrease in the sensing ability of the fibrous membrane was observed at higher degrees of relative humidity, which could be attributed to the adsorption of water molecules onto the PVA fibers, hindering their sensitivity to H_2S gas. These findings were previously observed when a non-fibrous PVA-based sensor film was evaluated [47]. Furthermore, the selectivity of the sensor was measured by exposing the sensor to various gasses, namely H_2, C_2H_6, NH_3, and NO_2 in addition to H_2S at an concentration of 300 ppm of each of the gasses. These gases were selected based on their chemical structure with various degrees of polarity. Despite the high polarity of NH_3 and NO_2 gases, their interaction with the PVA fibrous membrane was minimal. Results are shown in Fig. 10C, where the response time of the optimally fabricated WO_3 NPs-containing PVA sensor membrane was 18 times higher than other gasses used in this study, indicating its high selectivity to H_2S gas. Most significantly, Fig. 10D shows that the optimally fabricated sensor membrane is ultrasensitive to H2S gas with a capability of detecting 100 ppb at 40°C. It should be emntioned that previously described WO_3-based sensors have been reported to achieve similar low detection limits, but at very high temperatures (200-300^{o}C) [30, 40, 63, 64]. Thus, reducing the operating temperature from 200°C to 40°C saves

almost 90% of power consumed by the heating element of the sensor. This is based on the estimation of the percent power reduction using the following equation:

$$P_{reduction} = ([P_{200°C} - P_{40°C}]/ P_{200°C}) \times 100 \quad \text{(Eq. 3)}$$

Where $P_{200°C}$ and $P_{40°C}$ are the power consumed for sensing a fixed concentration of H_2S gas at 200 and 40^{o}C, respectively. The higher sensing efficiency of the optimally fabricated WO_3 NPs-containing PVA sensor membrane is highly attributed to the higher surface area of the PVA nanofibers, as compared with PVA non-fibrous films, which in turn provides an enhanced access of the entrapped WO_3 NPs to the H_2S gas at lower operating temperatures. It should be also mentioned that the presence of the ionic liquid further assists the sensing efficiency through its charged ions, which is also boosted due to its presence in a nm-size high surface area fibrous membrane. In addition, the non-woven nature of the PVA nanofibers provides a 3-dimensional network with interconnectivity and porosity which is believed to further facilitate the contacts between the WO_3 and IL within the fibers. A detailed comparison between the performance of our sensor versus already reported sensors in the literature are summarized in Table 1.

3.4. Gas sensing mechanism

In general, the change of sensor response arises from surface interactions between the target gas and sensing material. Therefore, understanding the sensing mechanism for WO_3 NPs embedded in a PVA NFs-based sensor membrane should consider: (i) the high surface area and porosity of the nanofiber which produces more reactive sites, and (ii) the adsorbed oxygen species (O_2^-, O^{2-} and O^-) onto the nanoparticle surface. The sensing mechanism in metal-oxide gas sensors depends on resistance change due to the adsorption of the target gas on the surface of

the sensing material. At first, the oxygen molecules easily adsorb on the surface of the sensing materiel due to the high electron affinity of the oxygen molecules (0.43 eV) [63]. The adsorbed oxygen molecules attract electrons from the PVA-WO_3 NFs surface. Consequently, adsorbed oxygen ions (O_2^-, O^- and O^{2-}) appear on the NFs surface. The following equations describe these reactions:

$$O_2(g) \rightarrow O_2(ads) \quad \text{(Eq.4)}$$

$$O_2(ads) + e^- \rightarrow O_2^-(ads) \quad \text{(Eq.5)}$$

$$O_2^-(ads) + e^- \rightarrow 2O^-(ads) \quad \text{(Eq.6)}$$

$$O^- + e^- \rightarrow O^{2-}(ads) \quad \text{(Eq.7)}$$

Upon exposure to H_2S gas, the adsorbed oxygen interacts with H_2S and free electrons are released as shown in the following equation.

$$2H_2S + 3O_2^- \rightarrow 2H_2O + 2SO_2 + 3\,e^- \quad \text{(Eq.8)}$$

The free electrons released from the above interaction increases the conductivity (decrease in resistance) of the nanofibers, and hence the current signal increases. This is further assisted by the nm-dimensions of the PVA fibers and the presence of the IL molecules. The high surface area of the PVA nanofibers enhances the extent of O_2 adsorption onto its surfaces, while the ionizable IL molecules facilitate the communication between the WO_3 NPs, hence improves current signal and the overall conductivity of the whole assembly. Upon turning off the H_2S flow, the density of free electrons is reduced and hence decreasing the conductivity of the sensing element causing a reversible sensing behavior [48]. The proposed optimally fabricated WO_3-PVA-IL fibrous sensor membrane, therefore, provides a novel formulation with an improved current pathway for H_2S gas detection utilizing, as compared with H_2S gas sensors that are commercially available or recently described in the literature.

4. Conclusion

This work demonstrates that high performance sensors can be fabricated using a hybrid organic-inorganic electrospun nanofibrous membranes for the detection of H_2S gas with the low ppb range. The sensing element of the H_2S sensor was produced by embedding WO_3 NPs in a nanofibrous PVA polymeric membrane together with glycerol as an ionic liquid. The effects of varying the spinning time, WO_3 NPs content and operating temperature on the sensing efficiency were investigated. Results revealed that the gas sensor fabricated with novel formulation exhibited exceptional H_2S sensing performance by detecting 1 ppm within 14.13 ± 2.29 s at room temperature. An optimally selected formulation of a PVA nanofibrous sensor membrane containing 7.5 wt% WO3 NPs, 5 vol% IL and electropsun for 9 hours was shown to have the highest detection performance at low temperature (20^{o}C), unlike WO3 NPs-based sensors that are described in the literature. With this novel formulation, we were able to detect 100 ppb of H_2S gas with a response time of 16.37 ± 1.42 s at 40°C. Moreover, the fabricated sensor assembly exhibited excellent reliability, long term stability and low power consumption, which are characteristics required by next generation gas sensing devices. As such, it offers an excellent potential to develop high performance H_2S sensing applications.

Journal Pre-proof

5. Acknowledgment

The authors would like to acknowledge the financial support by United Arab Emirates University with Grant Code: UPAR-G00002589 with Fund Code 31S310.

6. References

[1] D. W. Dockery, J. Schwartz, and J. D. Spengler, "Air pollution and daily mortality: associations with particulates and acid aerosols," *Environmental research*, vol. 59, pp. 362-373, 1992.

[2] G. Williams-Jones and H. Rymer, "Hazards of volcanic gases," in *The Encyclopedia of Volcanoes (Second Edition)*, ed: Elsevier, 2015, pp. 985-992.

[3] *Safety and Health Topics/Hydrogen Sulfide - Hazards. (n.d). Retrieved from:https://www.osha.gov/SLTC/hydrogensulfide/hazards.html.*

[4] K.-H. Kim, Y. Choi, E. Jeon, and Y. Sunwoo, "Characterization of malodorous sulfur compounds in landfill gas," *Atmospheric Environment*, vol. 39, pp. 1103-1112, 2005.

[5] K.-H. Kim, E.-C. Jeon, Y.-J. Choi, and Y.-S. Koo, "The emission characteristics and the related malodor intensities of gaseous reduced sulfur compounds (RSC) in a large industrial complex," *Atmospheric Environment*, vol. 40, pp. 4478-4490, 2006.

[6] K. Wetchakun, T. Samerjai, N. Tamaekong, C. Liewhiran, C. Siriwong, V. Kruefu, *et al.*, "Semiconducting metal oxides as sensors for environmentally hazardous gases," *Sensors and Actuators B: Chemical*, vol. 160, pp. 580-591, 2011.

[7] M. Kaur, N. Jain, K. Sharma, S. Bhattacharya, M. Roy, A. Tyagi, *et al.*, "Room-temperature H2S gas sensing at ppb level by single crystal In2O3 whiskers," *Sensors and Actuators B: Chemical*, vol. 133, pp. 456-461, 2008.

[8] Y.-y. Wang and Y.-x. Yang, "Effects of agriculture reclamation on the hydrologic characteristics in the Sanjiang Plain, China," *Chinese Geographical Science*, vol. 11, pp. 163-167, 2001.

[9] C. Yu, Y. Wang, K. Hua, W. Xing, and T. Lu, "Electrochemical H2S sensor with H2SO4 pre-treated Nafion membrane as solid polymer electrolyte," *Sensors and Actuators B: Chemical*, vol. 86, pp. 259-265, 2002.

[10] Y. Tanaka, T. Nakamoto, and T. Moriizumi, "Study of highly sensitive smell sensing system using gas detector tube combined with optical sensor," *Sensors and Actuators B: Chemical*, vol. 119, pp. 84-88, 2006.

[11] A. Sen, J. D. Albarella, J. R. Carey, P. Kim, and W. B. McNamara III, "Low-cost colorimetric sensor for the quantitative detection of gaseous hydrogen sulfide," *Sensors and Actuators B: Chemical*, vol. 134, pp. 234-237, 2008.

[12] M. T. S. Gomes, P. S. T. Nogueira, and J. A. Oliveira, "Quantification of CO2, SO2, NH3, and H2S with a single coated piezoelectric quartz crystal," *Sensors and Actuators B: Chemical*, vol. 68, pp. 218-222, 2000.

[13] F. He, X. Cui, and J. Ren, "A Novel QCM-based biosensor for detection of microorganisms producing hydrogen sulfide," *Analytical Letters*, vol. 41, pp. 2697-2709, 2008.

[14] R. Falconer, J. Vetelino, D. Smith, and M. Osborn, "An activation process for increased sensitivity of a SAW gas microsensor," in *Ultrasonics Symposium, ,* 1990, pp. 315-318.

[15] A. J. Heeger, "Semiconducting and metallic polymers: the fourth generation of polymeric materials," ed: ACS Publications, 2001, pp. 247-267.

[16] A. G. MacDiarmid, ""Synthetic metals": a novel role for organic polymers," *Current applied physics*, vol. 1, pp. 269-279, 2001.

[17] H. Shirakawa, "The discovery of polyacetylene film: The dawning of an era of conducting polymers," *Synthetic Metals*, vol. 125, pp. 3-10, 2001.

[18] T. Seiyama, A. Kato, K. Fujiishi, and M. Nagatani, "A new detector for gaseous components using semiconductive thin films," *Analytical Chemistry*, vol. 34, pp. 1502-1503, 1962.

[19] S. K. Pandey, K.-H. Kim, and K.-T. Tang, "A review of sensor-based methods for monitoring hydrogen sulfide," *TrAC Trends in Analytical Chemistry*, vol. 32, pp. 87-99, 2012.

[20] K. Crowley, A. Morrin, R. L. Shepherd, M. in het Panhuis, G. G. Wallace, M. R. Smyth, *et al.*, "Fabrication of polyaniline-based gas sensors using piezoelectric inkjet and screen printing for the detection of hydrogen sulfide," *IEEE Sensors Journal*, vol. 10, pp. 1419-1426, 2010.

[21] S. Virji, J. D. Fowler, C. O. Baker, J. Huang, R. B. Kaner, and B. H. Weiller, "Polyaniline nanofiber composites with metal salts: chemical sensors for hydrogen sulfide," *Small*, vol. 1, pp. 624-627, 2005.

[22] U. Lange, N. V. Roznyatovskaya, and V. M. Mirsky, "Conducting polymers in chemical sensors and arrays," *Analytica chimica acta,* vol. 614, pp. 1-26, 2008.

[23] M. Hanada, H. Koda, K. Onaga, K. Tanaka, T. Okabayashi, T. Itoh, *et al.*, "Portable oral malodor analyzer using highly sensitive In2O3 gas sensor combined with a simple gas chromatography system," *Analytica Chimica Acta,* vol. 475, pp. 27-35, 2003.

[24] J. Xu, X. Wang, and J. Shen, "Hydrothermal synthesis of In2O3 for detecting H2S in air," *Sensors and Actuators B: Chemical,* vol. 115, pp. 642-646, 2006.

[25] B. Esfandyarpour, S. Mohajerzadeh, A. A. Khodadadi, and M. D. Robertson, "Ultrahigh-sensitive tin-oxide microsensors for H/sub 2/S detection," *IEEE sensors journal,* vol. 4, pp. 449-454, 2004.

[26] I.-S. Hwang, J.-K. Choi, S.-J. Kim, K.-Y. Dong, J.-H. Kwon, B.-K. Ju, *et al.*, "Enhanced H2S sensing characteristics of SnO2 nanowires functionalized with CuO," *Sensors and Actuators B: Chemical,* vol. 142, pp. 105-110, 2009.

[27] A. Chowdhuri, V. Gupta, K. Sreenivas, R. Kumar, S. Mozumdar, and P. Patanjali, "Response speed of SnO 2-based H 2 S gas sensors with CuO nanoparticles," *Applied Physics Letters,* vol. 84, pp. 1180-1182, 2004.

[28] S. Steinhauer, E. Brunet, T. Maier, G. Mutinati, and A. Köck, "Suspended CuO nanowires for ppb level H2S sensing in dry and humid atmosphere," *Sensors and Actuators B: Chemical,* vol. 186, pp. 550-556, 2013.

[29] I. M. Szilágyi, S. Saukko, J. Mizsei, A. L. Tóth, J. Madarász, and G. Pokol, "Gas sensing selectivity of hexagonal and monoclinic WO3 to H2S," *Solid State Sciences,* vol. 12, pp. 1857-1860, 2010.

[30] N.-H. Kim, S.-J. Choi, D.-J. Yang, J. Bae, J. Park, and I.-D. Kim, "Highly sensitive and selective hydrogen sulfide and toluene sensors using Pd functionalized WO3 nanofibers for potential diagnosis of halitosis and lung cancer," *Sensors and Actuators B: Chemical,* vol. 193, pp. 574-581, 2014.

[31] L. Zhang, Z. Liu, L. Jin, B. Zhang, H. Zhang, M. Zhu, *et al.*, "Self-assembly gridding α-MoO3 nanobelts for highly toxic H2S gas sensors," *Sensors and Actuators B: Chemical,* vol. 237, pp. 350-357, 2016.

[32] L. Guo, N. Xie, C. Wang, X. Kou, M. Ding, H. Zhang, *et al.*, "Enhanced hydrogen sulfide sensing properties of Pt-functionalized α-Fe2O3 nanowires prepared by one-step electrospinning," *Sensors and Actuators B: Chemical*, vol. 255, pp. 1015-1023, 2018.

[33] Y. Wang, Y. Wang, J. Cao, F. Kong, H. Xia, J. Zhang, *et al.*, "Low-temperature H2S sensors based on Ag-doped α-Fe2O3 nanoparticles," *Sensors and Actuators B: Chemical*, vol. 131, pp. 183-189, 2008.

[34] S.-H. Wang, T.-C. Chou, and C.-C. Liu, "Nano-crystalline tungsten oxide NO2 sensor," *Sensors and Actuators B: Chemical*, vol. 94, pp. 343-351, 2003.

[35] J. Tamaki, K. Shimanoe, Y. Yamada, Y. Yamamoto, N. Miura, and N. Yamazoe, "Dilute hydrogen sulfide sensing properties of CuO–SnO2 thin film prepared by low-pressure evaporation method," *Sensors and Actuators B: Chemical*, vol. 49, pp. 121-125, 1998.

[36] P. Shewale, V. Patil, S. Shin, J. Kim, and M. Uplane, "H2S gas sensing properties of nanocrystalline Cu-doped ZnO thin films prepared by advanced spray pyrolysis," *Sensors and Actuators B: Chemical*, vol. 186, pp. 226-234, 2013.

[37] T.-t. Yu, X.-F. Zhang, Y.-M. Xu, X.-L. Cheng, S. Gao, H. Zhao, *et al.*, "Low concentration H2S detection of CdO-decorated hierarchically mesoporous NiO nanofilm with wrinkle structure," *Sensors and Actuators B: Chemical*, vol. 230, pp. 706-713, 2016.

[38] X. Liang, T.-H. Kim, J.-W. Yoon, C.-H. Kwak, and J.-H. Lee, "Ultrasensitive and ultraselective detection of H2S using electrospun CuO-loaded In2O3 nanofiber sensors assisted by pulse heating," *Sensors and Actuators B: Chemical*, vol. 209, pp. 934-942, 2015.

[39] A. Katoch, S.-W. Choi, J.-H. Kim, J. H. Lee, J.-S. Lee, and S. S. Kim, "Importance of the nanograin size on the H2S-sensing properties of ZnO–CuO composite nanofibers," *Sensors and Actuators B: Chemical*, vol. 214, pp. 111-116, 2015.

[40] J. Shi, Z. Cheng, L. Gao, Y. Zhang, J. Xu, and H. Zhao, "Facile synthesis of reduced graphene oxide/hexagonal WO3 nanosheets composites with enhanced H2S sensing properties," *Sensors and Actuators B: Chemical*, vol. 230, pp. 736-745, 2016.

[41] X. Gao, Y. Sun, C. Zhu, C. Li, Q. Ouyang, and Y. Chen, "Highly sensitive and selective H2S sensor based on porous ZnFe2O4 nanosheets," *Sensors and Actuators B: Chemical*, vol. 246, pp. 662-672, 2017.

[42] F. Huber, S. Riegert, M. Madel, and K. Thonke, "H2S sensing in the ppb regime with zinc oxide nanowires," *Sensors and Actuators B: Chemical*, vol. 239, pp. 358-363, 2017.

[43] Y. Kim, Y. S. Choi, S. Y. Park, T. Kim, S.-P. Hong, T. H. Lee, *et al.*, "Au decoration of a graphene microchannel for self-activated chemoresistive flexible gas sensors with substantially enhanced response to hydrogen," *Nanoscale*, vol. 11, pp. 2966-2973, 2019.

[44] H. Liu, M. Li, G. Shao, W. Zhang, W. Wang, H. Song, *et al.*, "Enhancement of hydrogen sulfide gas sensing of PbS colloidal quantum dots by remote doping through ligand exchange," *Sensors and Actuators B: Chemical*, vol. 212, pp. 434-439, 2015.

[45] N. Van Hoang, C. M. Hung, N. D. Hoa, N. Van Duy, and N. Van Hieu, "Facile on-chip electrospinning of ZnFe2O4 nanofiber sensors with excellent sensing performance to H2S down ppb level," *Journal of hazardous materials*, vol. 360, pp. 6-16, 2018.

[46] C. Wang, X. Chu, and M. Wu, "Detection of H2S down to ppb levels at room temperature using sensors based on ZnO nanorods," *Sensors and Actuators B: Chemical*, vol. 113, pp. 320-323, 2006.

[47] A. F. Abu-Hani, S. T. Mahmoud, F. Awwad, and A. I. Ayesh, "Design, fabrication, and characterization of portable gas sensors based on spinel ferrite nanoparticles embedded in organic membranes," *Sensors and Actuators B: Chemical*, vol. 241, pp. 1179-1187, 2017.

[48] A. F. Abu-Hani, F. Awwad, Y. E. Greish, A. I. Ayesh, and S. T. Mahmoud, "Design, fabrication, and characterization of low-power gas sensors based on organic-inorganic nano-composite," *Organic Electronics*, vol. 42, pp. 284-292, 2017.

[49] A. I. Ayesh, A. F. Abu-Hani, S. T. Mahmoud, and Y. Haik, "Selective H2S sensor based on CuO nanoparticles embedded in organic membranes," *Sensors and Actuators B: Chemical*, vol. 231, pp. 593-600, 2016.

[50] M. Allam, A. I. Ayesh, M. A. Mohsin, and Y. Haik, "Physical properties of PVA doped with algal glycerol," *Journal of Applied Polymer Science,* vol. 130, pp. 4482-4489, 2013.

[51] A. I. Ayesh, M. A. Mohsin, M. Y. Haik, and Y. Haik, "Investigations on electrical properties of poly (vinyl alcohol) doped with 1-methyl-3-n-decyl-imidazolium bromide ionic liquid," *Current Applied Physics,* vol. 12, pp. 1223-1228, 2012.

[52] D. Wei and A. Ivaska, "Applications of ionic liquids in electrochemical sensors," *Analytica Chimica Acta,* vol. 607, pp. 126-135, 2008.

[53] J.-H. Kim, A. Mirzaei, Y. Zheng, J.-H. Lee, J.-Y. Kim, H. W. Kim, *et al.*, "Enhancement of H2S sensing performance of p-CuO nanofibers by loading p-reduced graphene oxide nanosheets," *Sensors and Actuators B: Chemical,* vol. 281, pp. 453-461, 2019.

[54] M. Zhao, X. Wang, L. Ning, J. Jia, X. Li, and L. Cao, "Electrospun Cu-doped ZnO nanofibers for H2S sensing," *Sensors and Actuators B: Chemical,* vol. 156, pp. 588-592, 2011.

[55] N. A. Hotaling, K. Bharti, H. Kriel, and C. G. Simon, "DiameterJ: A validated open source nanofiber diameter measurement tool," *Biomaterials,* vol. 61, pp. 327-338, 2015.

[56] J. H. Park, M. R. Karim, I. K. Kim, I. W. Cheong, J. W. Kim, D. G. Bae, *et al.*, "Electrospinning fabrication and characterization of poly (vinyl alcohol)/montmorillonite/silver hybrid nanofibers for antibacterial applications," *Colloid and Polymer Science,* vol. 288, pp. 115-121, 2010.

[57] R. Augustine, H. N. Malik, D. K. Singhal, A. Mukherjee, D. Malakar, N. Kalarikkal, *et al.*, "Electrospun polycaprolactone/ZnO nanocomposite membranes as biomaterials with antibacterial and cell adhesion properties," *Journal of Polymer Research,* vol. 21, p. 347, 2014.

[58] V. Gimenez, A. Mantecon, and V. Cadiz, "Modification of poly (vinyl alcohol) with acid chlorides and crosslinking with difunctional hardeners," *Journal of Polymer Science Part A: Polymer Chemistry,* vol. 34, pp. 925-934, 1996.

[59] S. Park, S. Park, J. Jung, T. Hong, S. Lee, H. W. Kim, *et al.*, "H2S gas sensing properties of CuO-functionalized WO3 nanowires," *Ceramics International*, vol. 40, pp. 11051-11056, 2014.

[60] G. Korotcenkov, "Metal oxides for solid-state gas sensors: What determines our choice?," *Materials Science and Engineering: B*, vol. 139, pp. 1-23, 2007.

[61] Y. Gui, F. Dong, Y. Zhang, Y. Zhang, and J. Tian, "Preparation and gas sensitivity of WO3 hollow microspheres and SnO2 doped heterojunction sensors," *Materials Science in Semiconductor Processing*, vol. 16, pp. 1531-1537, 2013.

[62] W. Mickelson, A. Sussman, and A. Zettl, "Low-power, fast, selective nanoparticle-based hydrogen sulfide gas sensor," *Applied Physics Letters*, vol. 100, pp. 173110 (1-4), 2012.

[63] S. Bai, K. Zhang, J. Sun, D. Zhang, R. Luo, D. Li, *et al.*, "Polythiophene-WO3 hybrid architectures for low-temperature H2S detection," *Sensors and Actuators B: Chemical*, vol. 197, pp. 142-148, 2014.

[64] S.-J. Choi, F. Fuchs, R. Demadrille, B. Grévin, B.-H. Jang, S.-J. Lee, *et al.*, "Fast responding exhaled-breath sensors using WO3 hemitubes functionalized by graphene-based electronic sensitizers for diagnosis of diseases," *ACS applied materials & interfaces*, vol. 6, pp. 9061-9070, 2014.

[65] A. Mane, M. Suryawanshi, J. Kim, and A. Moholkar, "Highly selective and sensitive response of 30.5% of sprayed molybdenum trioxide (MoO3) nanobelts for nitrogen dioxide (NO2) gas detection," *Journal of colloid and interface science*, vol. 483, pp. 220-231, 2016.

7. Figures and tables captions:

Fig. 1 H_2S gas testing system.

Fig. 2 XRD patterns (A) and SEM micrograph (B) of the as-received WO_3 NPs.

Fig. 3 SEM images of A) PVA-5vol%IL-5wt%WO_3-5H B) PVA-5vol%IL-5wt%WO_3-7H C) PVA-5vol%IL-5wt%WO_3-9H D) Porosity and thickness variation with spinning time

Fig. 4 SEM images of A) Pristine PVA nanofibers B) PVA-5vol%IL-5wt%WO_3-9H C) PVA-5vol%IL-7.5wt%WO_3-9H D) PVA-5vol%IL-10wt%WO_3-9H E) Porosity and fiber variation with WO_3 content F) EDX of PVA-5vol%IL-7.5wt%WO_3-9H.

Fig. 5 Thermograms of the as-received PVA pellets and the electrospun PVA NFs.

Fig. 6 A) I-V characteristic curve of (PVA-5vol%IL-7.5wt%WO_3-9H) sensor as a function of temperature B) The dependence of the natural logarithm of the resistance on inverse temperature for the PVA-5vol%IL-7.5wt%WO_3-9H.

Fig. 7 Reproducibility and Representative measuring curve of PVA-5vol%IL-7.5wt%WO_3-9H sensor for A) 1 ppm at 20°C B) 100 ppb at 40°C.

Fig. 8 PVA-5vol%IL-5wt%WO_3-5-9H sensor response at (A) 40°C (B) 60°C for different spinning time.

Fig. 9 PVA-5vol%IL-5-10wt%WO_3-9H sensor response at (A)20°C (B)40°C and (C)60°C (D) Variation of response time of PVA-5vol%IL-7.5wt%WO_3-9H with temperature.

Fig. 10 A: Long term stability of PVA-5vol%IL-7.5wt%WO_3-9H sensor B) Humidity effect on PVA-5vol%IL-7.5wt%WO_3-9H sensor C) Selectivity of PVA-5vol%IL-7.5wt%WO_3-9H sensor D) detection limit of PVA-5vol%IL-7.5wt%WO_3-9H sensor at 40°C.

Table 1 Comparison between the performance of our sensor and other recently developed H_2S gas sensors.

Journal Pre-proof

Table 1

Material	Structure	Detection limit	Response Value (%)	Operation temperature (^{O}C)	Reference
PVA-IL-WO_3	Nanofibers	100 ppb	12.54 for 1 ppm	40	Present work
PVA-IL-WO_3		1 ppm		20	Present work
PVA-WO_3	Thin film	15 ppm	-	20	[48]
Reduced graphene oxide/hexagonal WO_3	Nano sheets	10 ppb	168.5 for 40 ppm	330	[40]
Pd-NPs/Pd-embedded WO_3	NFs	1 ppm	1.36 for 1 ppm	350	[30]
Pristine WO_3 NFs			11.1 for 1 ppm		
Polythiophene-WO3	Nano sheet	2 ppm	3 for 10 ppm	70	[63]
WO_3 hemitube functionalized with graphene-based material	Hemitubes	100 bbp	-	200-300	[64]

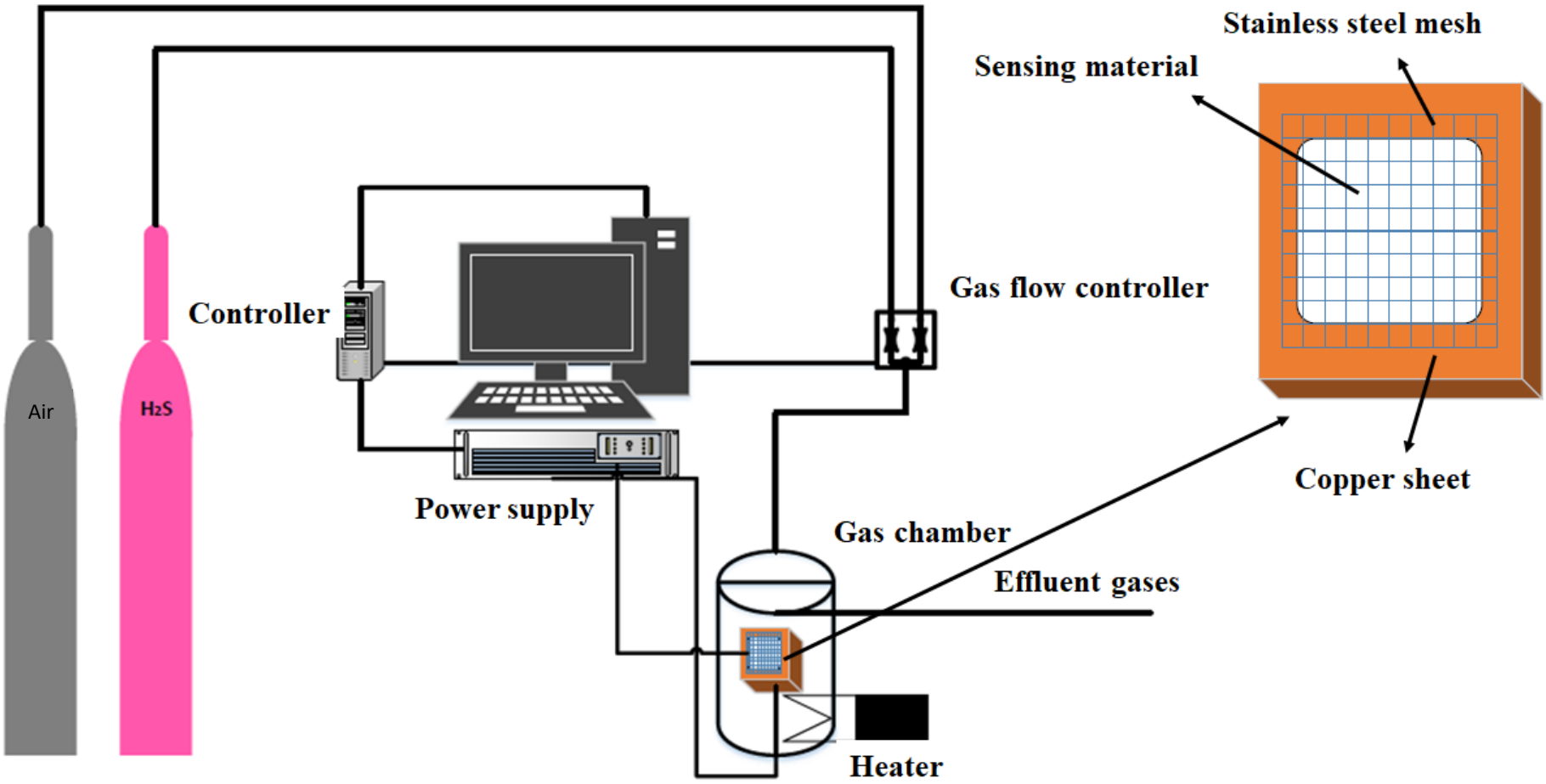
Stainless steel mesh
Sensing material
Gas flow controller
Controller
Air
H2S
Power supply
Copper sheet
Gas chamber
Effluent gases
Heater

Figure 1

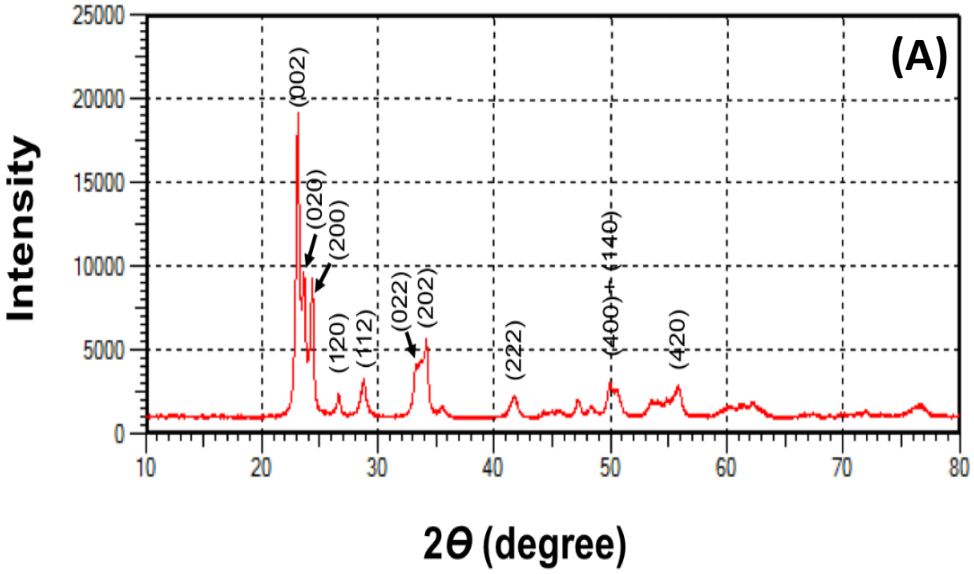
(A)
Intensity
2θ (degree)
(002)
(020)
(200)
(120)
(112)
(022)
(202)
(222)
(400)+ (140)
(420)

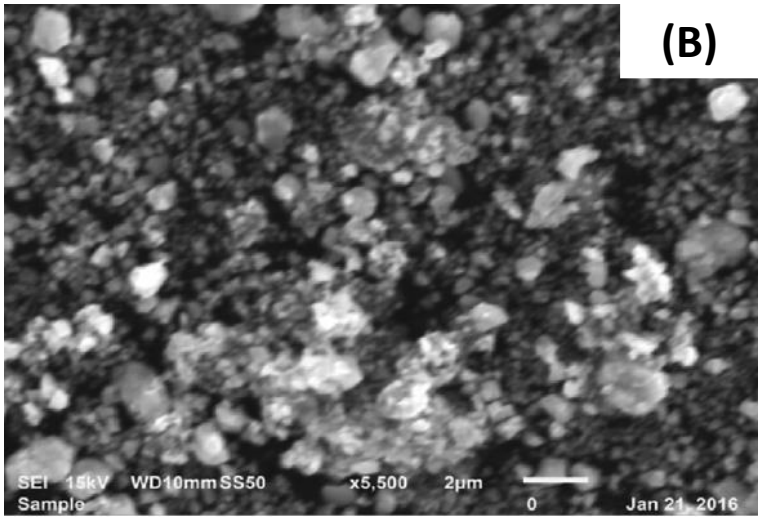
(B)
SEI 15kV WD10mm SS50 x5,500 2μm
Sample
0
Jan 21, 2016

Figure 2

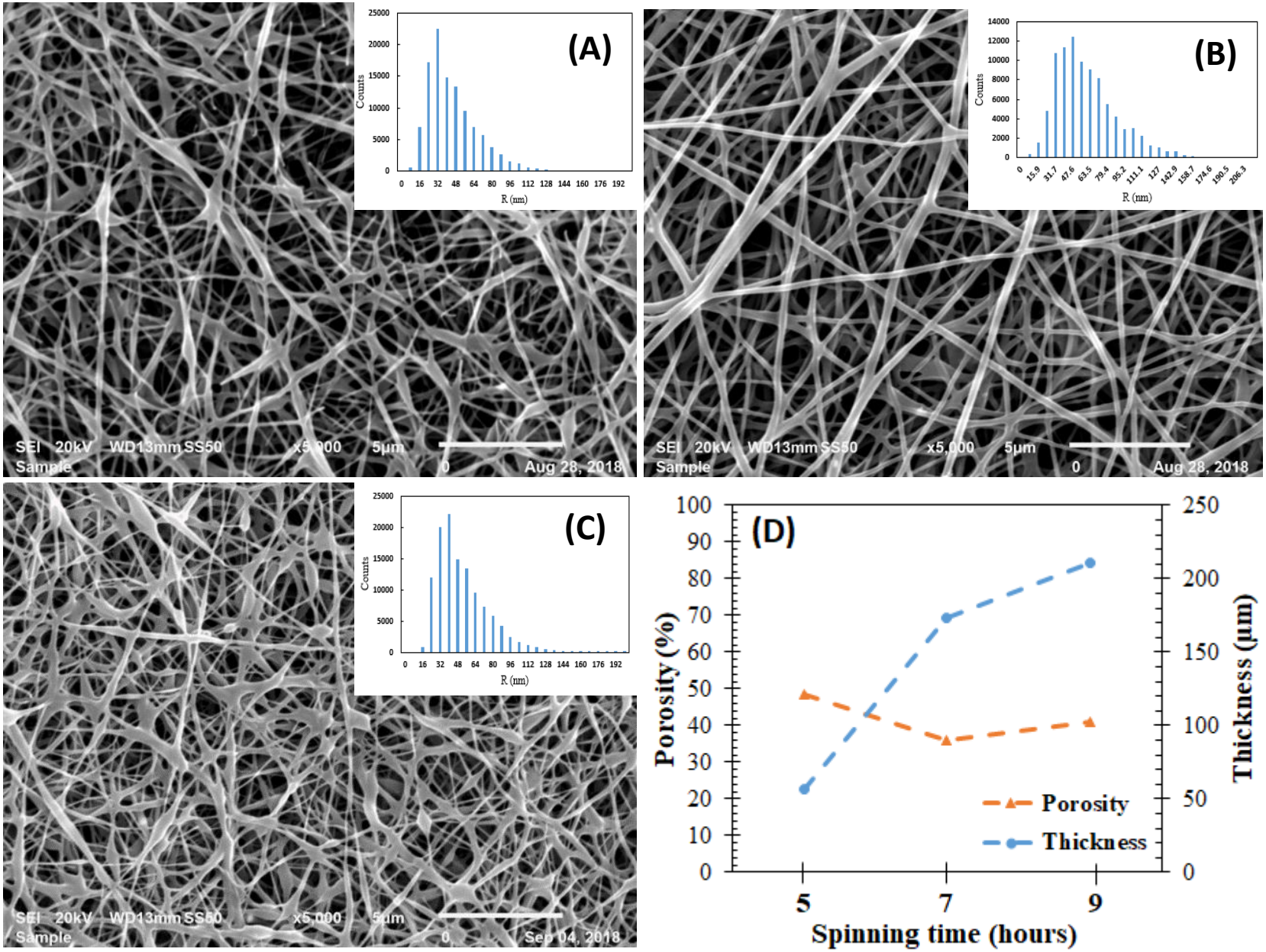
(A)
Counts
R (nm)
SEI 20kV WD13mm SS50 x5,000 5µm
Sample
Aug 28, 2018
(B)
Counts
R (nm)
SEI 20kV WD13mm SS50 x5,000 5µm
Sample
Aug 28, 2018
(C)
Counts
R (nm)
SEI 20kV WD13mm SS50 x5,000 5µm
Sample
Sep 04, 2018
(D)
Porosity (%)
Thickness (µm)
Porosity
Thickness
Spinning time (hours)

Figure 3

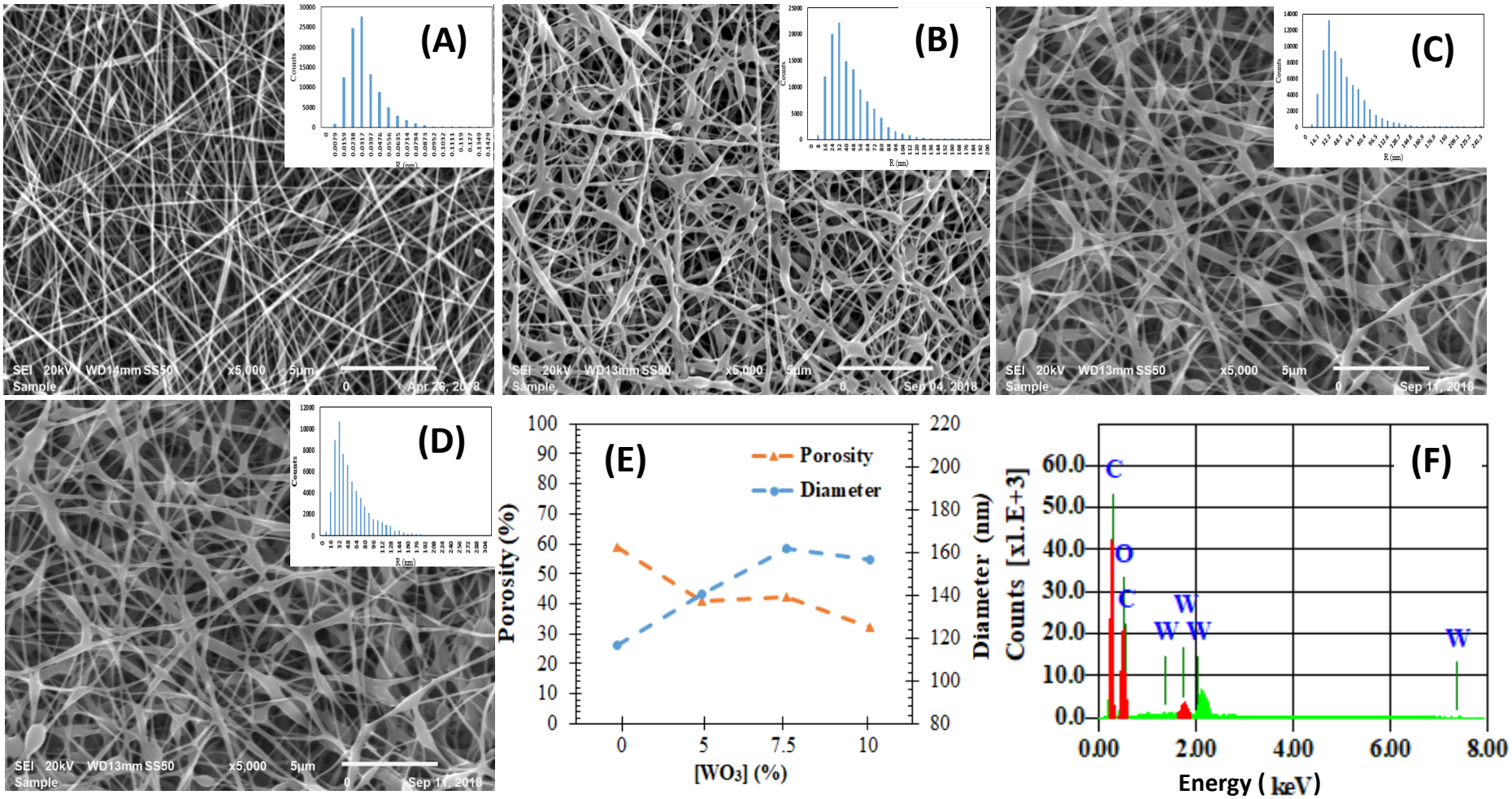
(A)
(B)
(C)
(D)
(E)
(F)
Porosity
Diameter
Porosity (%)
Diameter (nm)
[WO3] (%)
Counts [x1.E+3]
Energy (keV)
C
O
W

Figure 4

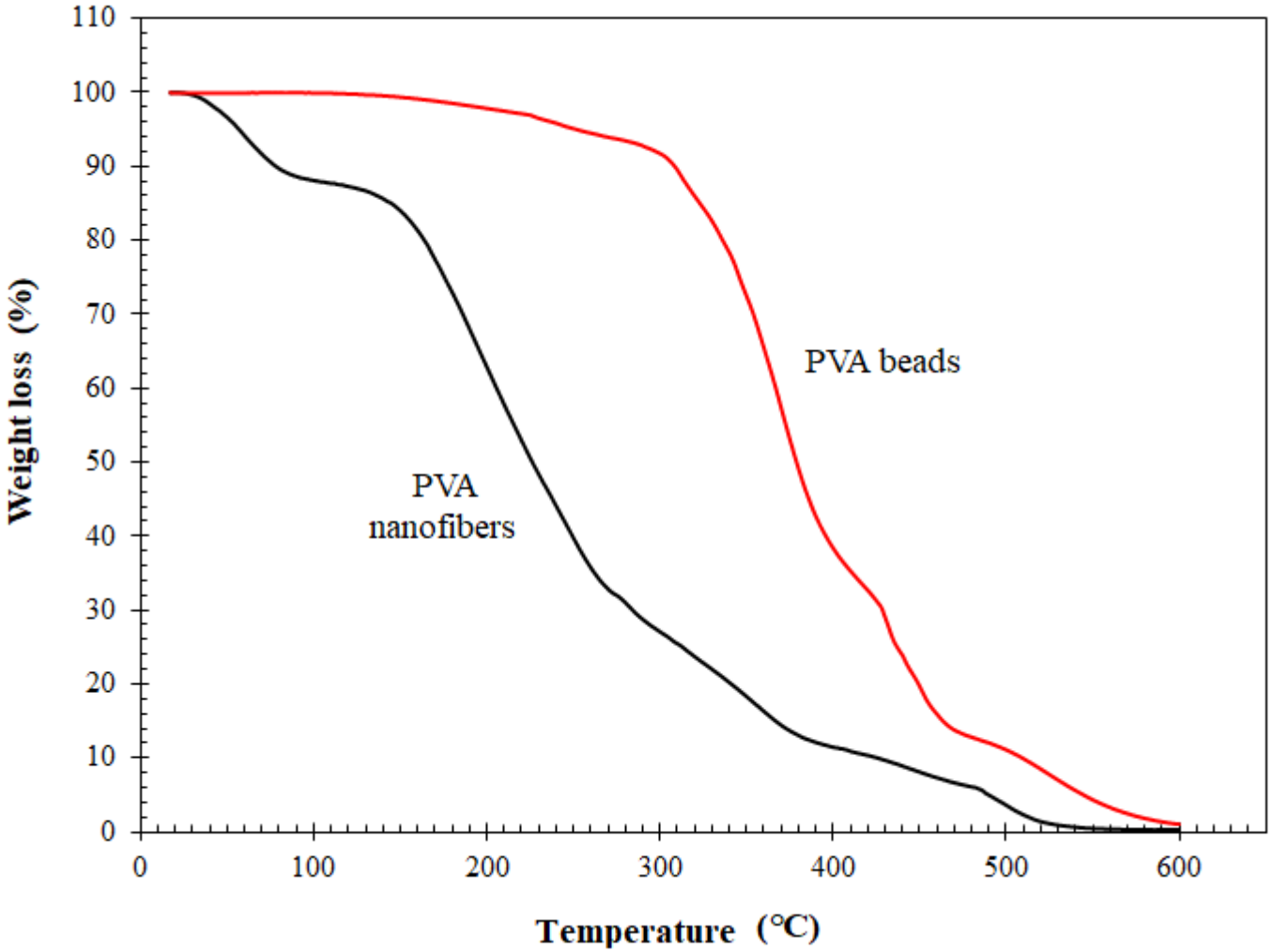
Weight loss (%)
110
100
90
80
70
60
50
40
30
20
10
0
0
100
200
300
400
500
600
Temperature (°C)
PVA beads
PVA
nanofibers

Figure 5

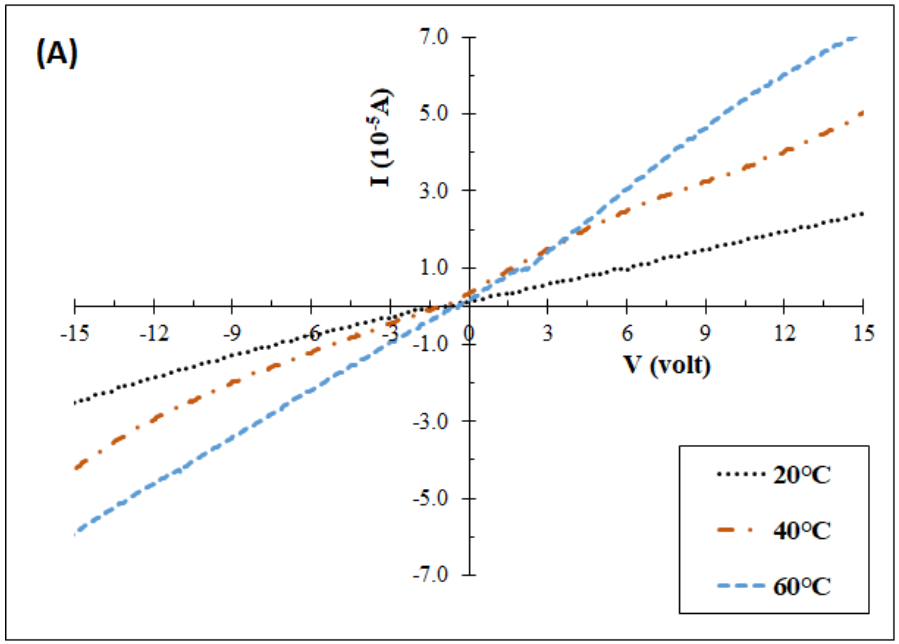
(A)
I (10-5A)
7.0
5.0
3.0
1.0
-1.0
-3.0
-5.0
-7.0
-15
-12
-9
-6
-3
0
3
6
9
12
15
V (volt)
20°C
40°C
60°C

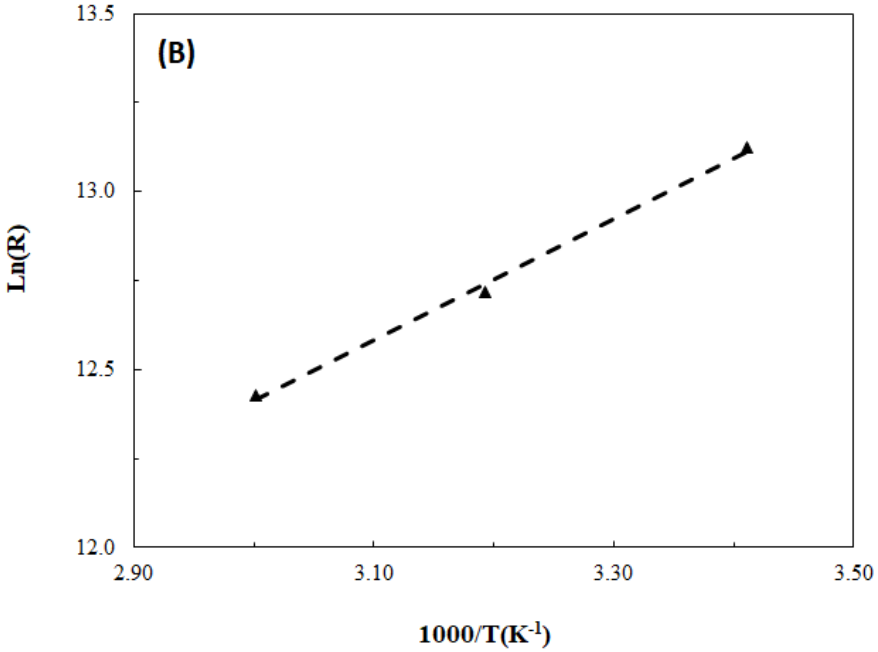
(B)
Ln(R)
13.5
13.0
12.5
12.0
2.90
3.10
3.30
3.50
1000/T(K-1)

Figure 6

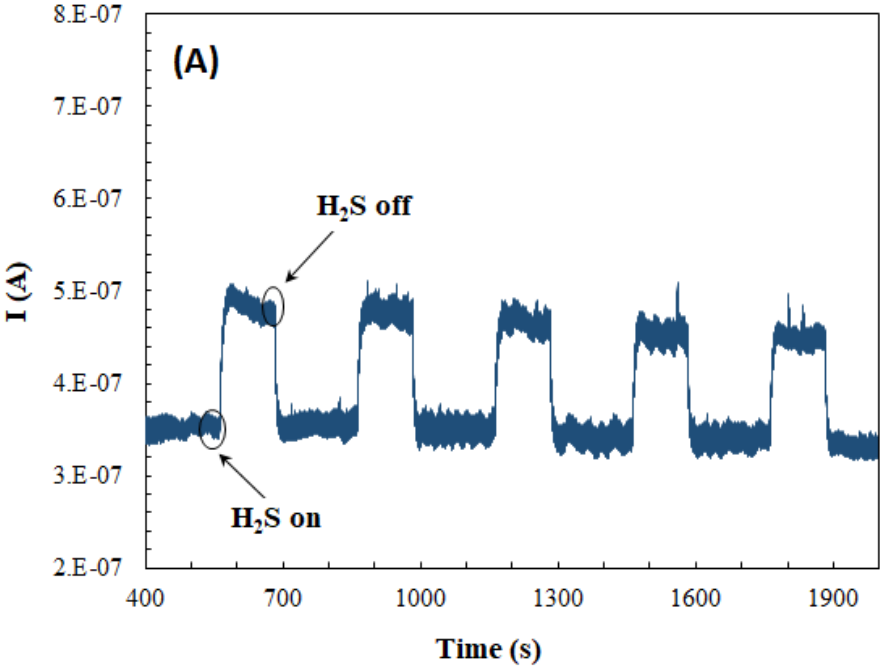
(A)
8.E-07
7.E-07
6.E-07
5.E-07
4.E-07
3.E-07
2.E-07
I (A)
H2S off
H2S on
400
700
1000
1300
1600
1900
Time (s)

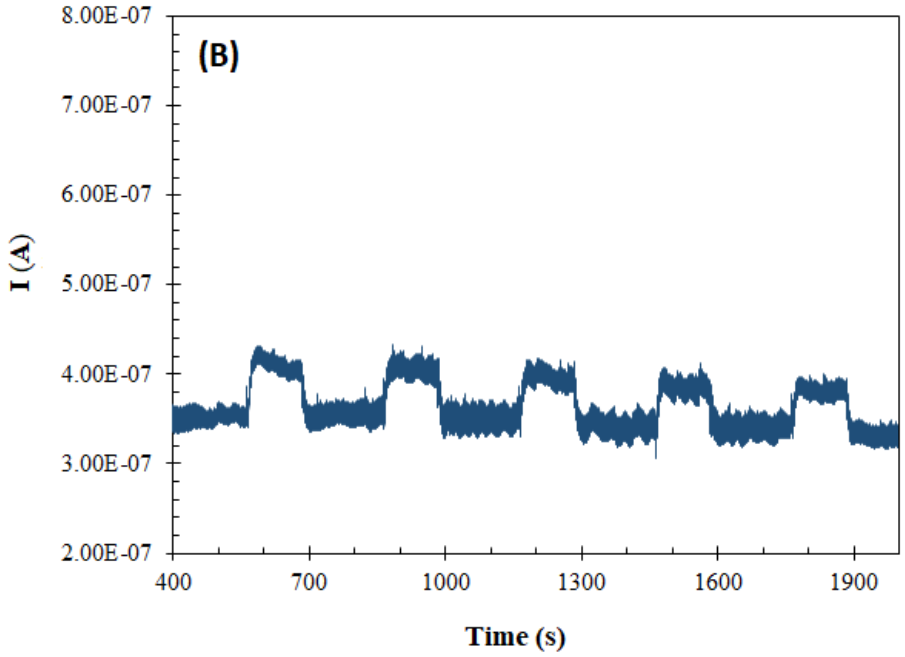
(B)
8.00E-07
7.00E-07
6.00E-07
5.00E-07
4.00E-07
3.00E-07
2.00E-07
I (A)
400
700
1000
1300
1600
1900
Time (s)

Figure 7

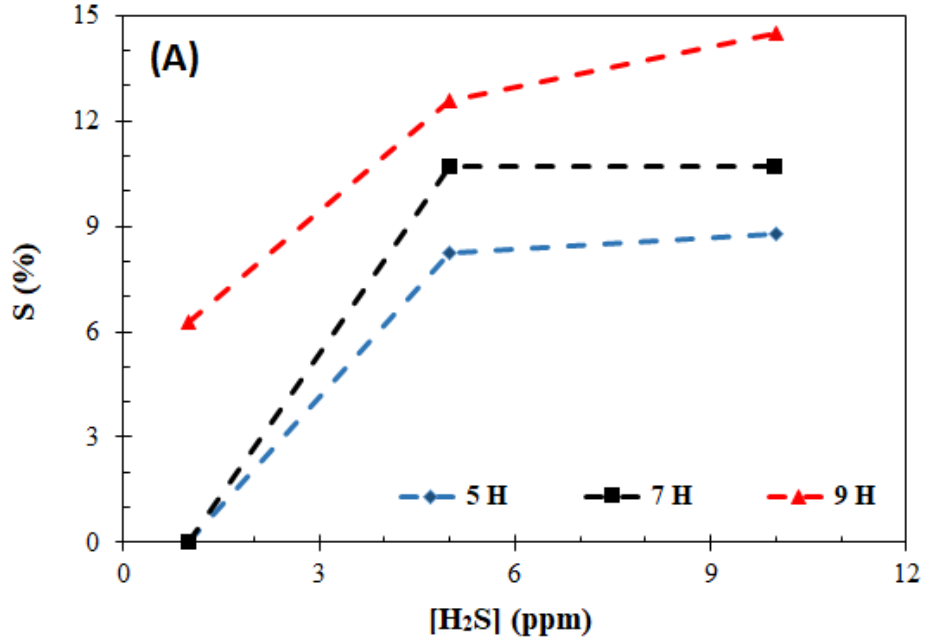
(A)
15
12
9
6
3
0
S (%)
0
3
6
9
12
[H2S] (ppm)
5 H
7 H
9 H

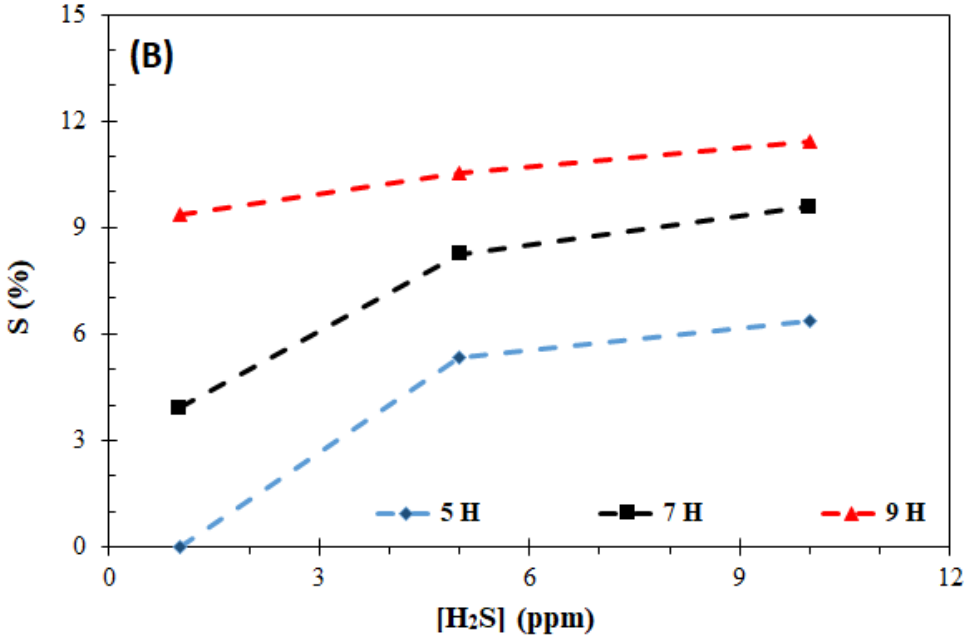
(B)
15
12
9
6
3
0
S (%)
0
3
6
9
12
[H2S] (ppm)
5 H
7 H
9 H

Figure 8

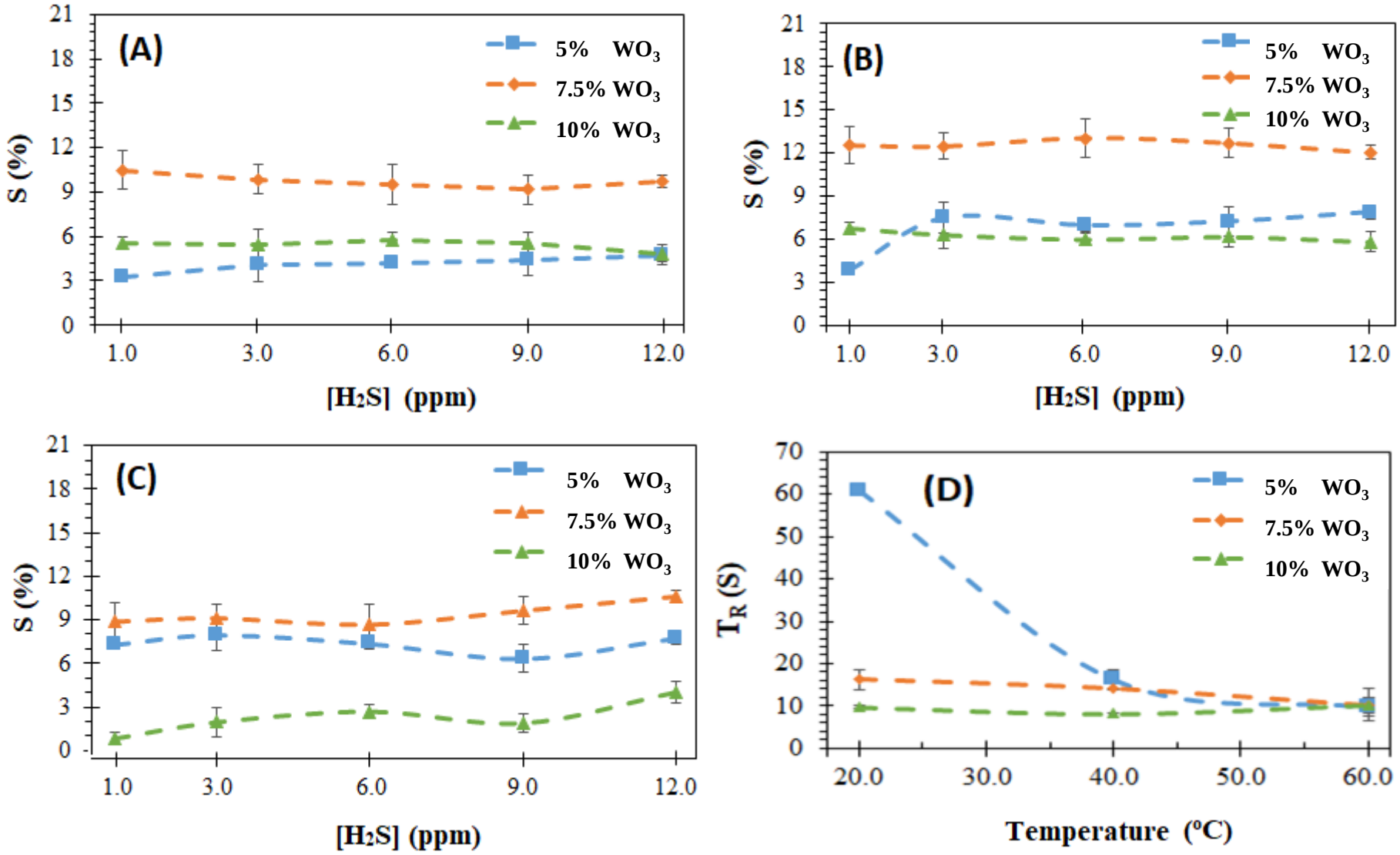
(A)
5% WO3
7.5% WO3
10% WO3
S (%)
[H2S] (ppm)
(B)
5% WO3
7.5% WO3
10% WO3
S (%)
[H2S] (ppm)
(C)
5% WO3
7.5% WO3
10% WO3
S (%)
[H2S] (ppm)
(D)
5% WO3
7.5% WO3
10% WO3
TR (S)
Temperature (°C)

Figure 9

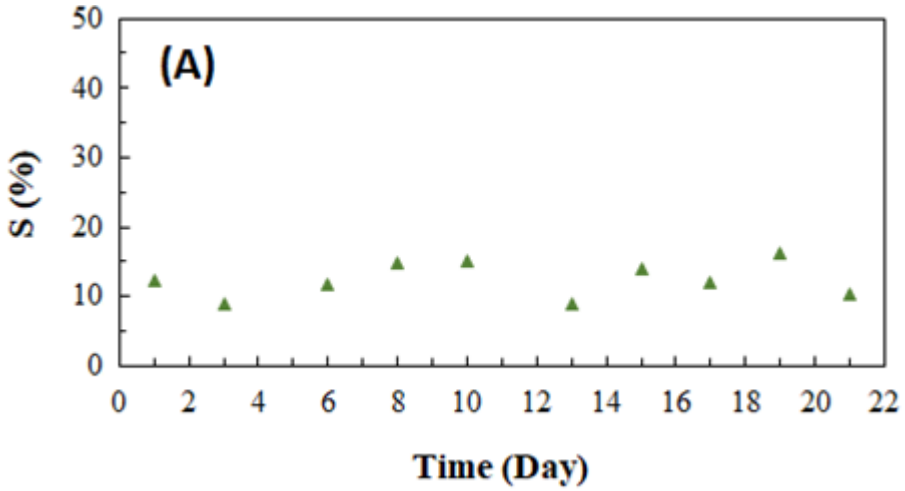
(A)
S (%)
Time (Day)

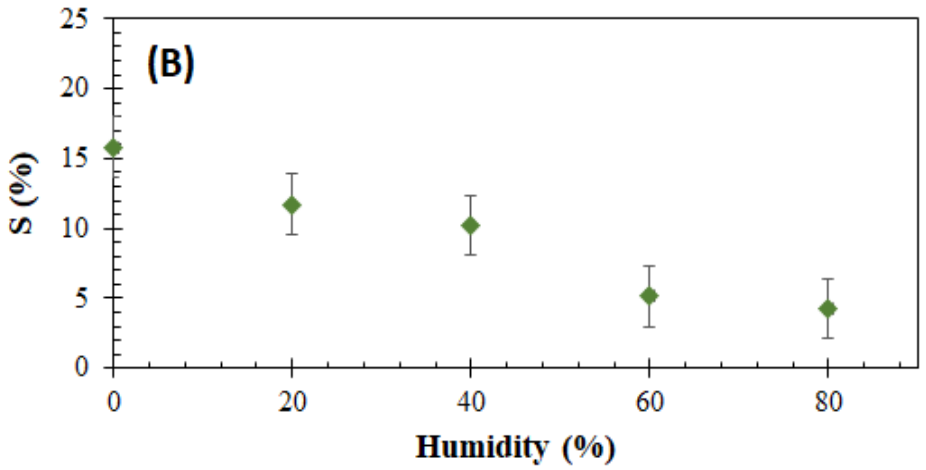
(B)
S (%)
Humidity (%)

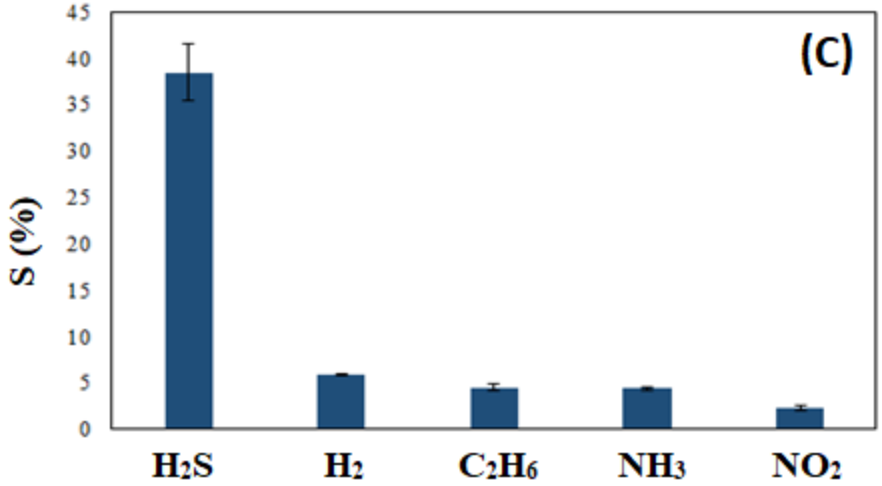
(C)
S (%)
H2S
H2
C2H6
NH3
NO2

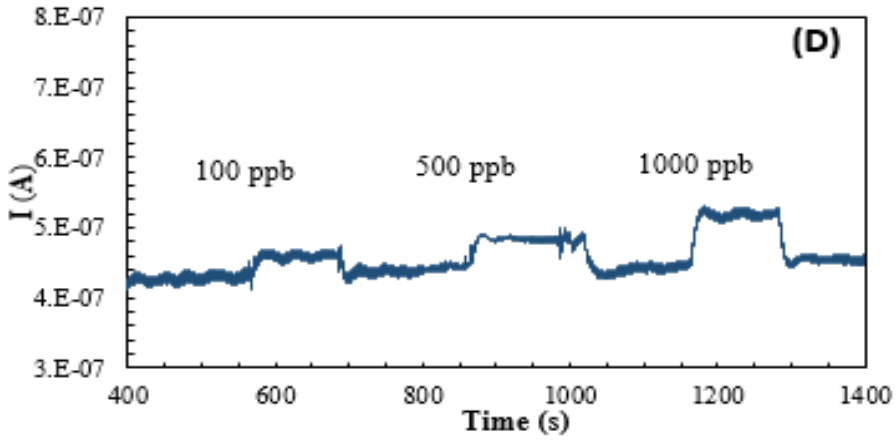
(D)
I (A)
100 ppb
500 ppb
1000 ppb
Time (s)

Figure 10

Table 1

Material	Structure	Detection limit	Response Value (%)	Operation temperature (^{O}C)	Reference
PVA-IL-WO_3	Nanofibers	100 ppb	12.54 for 1 ppm	40	Present work
PVA-IL-WO_3		1 ppm		20	Present work
PVA-WO_3	Thin film	15 ppm	-	20	[48]
Reduced graphene oxide/hexagonal WO_3	Nano sheets	10 ppb	168.5 for 40 ppm	330	[40]
Pd-NPs/Pd-embedded WO_3	NFs	1 ppm	1.36 for 1 ppm	350	[30]
Pristine WO_3 NFs			11.1 for 1 ppm		
Polythiophene-WO3	Nano sheet	2 ppm	3 for 10 ppm	70	[63]
WO_3 hemitube functionalized with graphene-based material	Hemitubes	100 bbp	-	200-300	[64]

Journal Pre-proof

Research Highlights

1. Organic-Inorganic nanofibers based gas sensors were successfully prepared by electrospinning for the first time.

2. The prepared organic-inorganic gas sensor could detect 100 ppb of H_2S gas at a very low temperature (40^oC).

3. The fabricated sensor is very selective with fast response time of 16.37 s.

4. The sensor is having long-term stability and low power consumption.

Journal Pre-proof

Department of Physics **Jan 21, 2020**

To: Organic Electronics

Ms. Ref. No.: ORGELE-D-19-01026

On behalf of all Authors of this manuscript **Ms. Ref. No.: ORGELE-D-19-01026**, we declare that we have no financial and personal relationships with other people or organizations that could influence and bias their work. **There are no interests to declare.**

MAHMOUD

Corresponding author:
Saleh Thaker Mahmoud, PhD
Professor of Physics
Department of Physics
UAE University, P. O. Box.15551 Al-Ain
United Arab Emirates
E-mail: saleh.thaker@uaeu.ac.ae

Journal Pre-proof